PTEP

Prog. Theor. Exp. Phys. **2021**, 113D01 (20 pages)
DOI: 10.1093/ptep/ptab120

Formulation of a shell–cluster overlap integral with the Gaussian expansion method

R. Nakamoto[1], E. Ueda[1], M. Ito[1,2,*], and N. Shimizu[3]

[1]*Department of Pure and Applied Physics, Kansai University, 3-3-35 Yamatecho, Suita 564-8680, Japan*
[2]*Research Center for Nuclear Physics (RCNP), Osaka University, 10-1 Mihogaoka, Suita 567-0047, Japan*
[3]*Center for Nuclear Study, The University of Tokyo, 7-3-1 Hongo, Bunkyo-ku, Tokyo 113-0033, Japan*
*E-mail: itomk@kansai-u.ac.jp

Received June 13, 2021; Revised September 1, 2021; Accepted September 15, 2021; Published September 23, 2021

We formulate a computational method to evaluate the overlap integral of the shell-model and cluster-model wave functions. The framework is applied to the system of the core plus two neutrons, and the magnitude of the overlap of the shell-model configuration (core + n + n) and the di-neutron cluster one (core + $2n$) is explored. We have found that the magnitude of the overlap integral is prominently enhanced when two neutrons occupy shell-model orbits with low orbital angular momenta, such as s- and p-wave orbits. The shell–cluster overlap is calculated in systems with jj-closed cores plus two neutrons, and the enhancement due to occupation of the s or p orbit also occurs in the systematic calculation. The effect of the configuration interaction on the shell–cluster overlap integrals is also discussed.

Subject Index D11, D13

1. Introduction

The nuclear shell model and the mean-field model are standard models to describe ground and low-lying states in nuclear systems [1–4]. In the ground state of a nucleus, all nucleons contribute to generating a mean field in a self-consistent manner, and they show independent particle motion by occupying single-particle orbits in a self-consistent mean field (see Ref. [1] and references therein). There are energy gaps in a sequence of single-particle orbits; this level structure is called the shell structure [1–4]. The nuclear shell model, which considers single-particle configurations based on the shell structure, is quite successful in explaining the ground-state properties of nuclei over a wide mass region, except for a few examples [1–4].

In contrast, in lighter mass systems, there appear clustering phenomena, in which several nucleons are spatially localized and form subunits called clusters. A typical well known example of such a cluster is the α cluster [5–7], which is a quartet of two protons and two neutrons. In most of the ground states of nuclear systems, the α cluster and the residual nucleus are merged, which leads to the formation of a compound system with the shell structure, but α clustering is greatly enhanced in particular excited states [5–7]. Furthermore, in recent studies, di-neutron correlations have been extensively investigated in lighter mass regions [8–11]. Two neutrons do not form a bound state in free space but the spatial localization of the di-neutron around a nuclear surface has been confirmed experimentally [8,9] and compared with theoretical calculations [10,11].

The independent particle configuration in the shell model seems to contradict the cluster configuration with the spatial localization of the nucleons but these two configurations are non-orthogonal, and hence the amplitude of the cluster formation is non-zero even if the pure shell-model structure

is realized, in which the individual nucleons show completely independent particle motions. The relationship between the shell-model and the α-cluster-model configurations has been discussed in detail in the lighter mass region, where the spin–orbit interaction is ineffective [5,7] (see also Refs. [6,12] and references therein). However, the relationship between the shell–cluster configurations remains unclear in the heavy mass region, in which the spin–orbit interaction must be prominent due to the occupation of shell-model orbits with higher orbital angular momenta (see Ref. [1] and references therein).

The evaluation of the non-orthogonal amplitude of the shell and cluster models is important to clarify the relationship between these two models, which seem to describe the different particle motions intuitively. The non-orthogonal amplitude can be directly calculated by the overlap integral of the wave functions in the shell and cluster models, which are defined by multi-dimensional integration involving coordinate rearrangements [13,14]. It is interesting and instructive to explore the systematic features of the shell–cluster overlap integral in systems of a core plus valence nucleons, which can be obtained by varying the valence orbits, the core mass number, the spatial size of the cluster, and so on.

In this article, we formulate a new method to calculate the overlap integral of the wave functions in the shell and cluster models by combining the Gaussian expansion method (GEM) [13–16] with the Fourier transformation (FT). The new framework of GEM + FT is applied to core-plus-two-neutrons systems, and we investigate the basic features of the overlap integrals of the naive shell-model configuration and the di-neutron cluster one. Furthermore, a calculation of the configuration interaction (CI) is also performed [2,3,17], and the CI effect on the shell–cluster overlap integral is systematically investigated. Although we focus on a discussion of the core-plus-two-neutrons system in the present article, the new framework can also be extended to a core-plus-four-nucleons system, corresponding to a core-plus-α-cluster system, in a straightforward manner.

The matrix elements of the shell and cluster configurations can also be transformed by the traditional method in the shell-model calculation, the Talmi–Moshinsky (TM) transformation [18,19], and we can see its recent application in Ref. [20]. The TM transformation can be applied to the transformation using the harmonic oscillator (HO) basis function with a common length parameter, $\hbar\omega$. Numerically, the superposition of HO bases with different nodal numbers makes it difficult to optimize the oscillator length $\hbar\omega$ from a set of solutions with different $\hbar\omega$ in the calculation of weakly bound or unbound resonant states [21], where a tail of the wave functions is prominently extended to the outer region of the nuclear interaction. Thus, computational methods using HO expansion are not so convenient for analyzing cluster correlations in extremely weakly bound systems, e.g., di-neutron correlations [8–11].

In contrast, superpositions of the Gaussian bases employed in GEM can describe the spatially extended wave functions in weakly bound systems [13,14,22]. In the calculation of the unbound states, a detailed comparison of GEM with the Gamow shell model relying on HO expansion is discussed in Ref. [22], and it demonstrates a clear convergence of the resonant solution in GEM. Moreover, GEM is also able to handle highly oscillating wave functions, which widely appear from the bound states [13,15,16] to the unbound states [23,24], by extending the real range parameter to the complex range one. Such highly oscillating features in the wave function really appear in the α-cluster structure inside a heavy nucleus [5–7,25]. Therefore, GEM is more flexible and applicable than the computational method with HO expansion.

We combine GEM and the Fourier transformation (FT) in the calculation of the overlap integral. The method of GEM + FT can be extended to the computation of any matrix elements for one-body

and two-body operators expressed in terms of the nucleon degrees of freedom because the shell–cluster matrix elements in the Fourier representation can be handled in a similar manner to the mathematical technique using the so-called overlap matrix or B-matrix [7].

The organization of this article is as follows. In Sect. 2, the framework to calculate the shell–cluster overlap integrals by Fourier transformation is explained. In Sect. 3, the results of the calculated overlap of the core-plus-two-neutrons systems are presented. We discuss the basic features of the overlap integral by varying the valence orbits and the sizes of the di-neutron clusters. Systematic calculations of the shell–cluster overlap are done by varying the core nucleus. The CI effect on the shell–cluster overlap is also investigated systematically. The final section is devoted to the summary and discussion.

2. Theoretical framework

We formulate the computational method of the shell–cluster overlap integrals for a two-nucleon configuration around a heavy inert core. In this section, we explain the main framework to compute the overlap integrals; the detailed derivation process of the overlap integrals is described in the appendix.

2.1. *Model wave functions*

The explicit expression for the single-particle orbit ϕ in the jj-coupling scheme around the core nucleus is

$$\phi^{(\tau)}_{nl\frac{1}{2}jj_z}(\boldsymbol{r},\boldsymbol{\xi},\boldsymbol{\eta}) = R_{nlj}(r)\left[Y_l(\hat{\boldsymbol{r}})\otimes \upsilon_{1/2}(\boldsymbol{\xi})\right]_{jj_z}\Upsilon_\tau(\boldsymbol{\eta}), \tag{1}$$

where the wave functions of $R_{nlj}(r)$, $Y_l(\hat{\boldsymbol{r}})$, $\upsilon_{1/2}(\boldsymbol{\xi})$, $\Upsilon_\tau(\boldsymbol{\eta})$ denote the radial, angular, spin, and isospin parts, respectively. The respective arguments in these functions are the position vector $\boldsymbol{r} = (r, \hat{\boldsymbol{r}})$, the spin coordinate $\boldsymbol{\xi}$, and the isospin coordinate $\boldsymbol{\eta}$. The single-particle orbit is specified by the principal quantum number (or number of the radial node) n, the orbital angular momentum l, the nucleon spin $1/2$, the total angular momentum j, and its third component j_z. τ specifies the third component of the isospin for the nucleon, such as a proton ($\tau = p$) or a neutron ($\tau = n$).

In the shell model, the wave function of the M-scheme basis state for two nucleons with an inert core is described as a Slater determinant of two single-particle wave functions and written as

$$\Psi_s = N\mathcal{A}\left\{\phi^{(\tau_1)}_{a_1}(\boldsymbol{r}_1)\phi^{(\tau_2)}_{a_2}(\boldsymbol{r}_2)\right\}. \tag{2}$$

Here $\phi^{(\tau_i)}_a(\boldsymbol{r}_i)$ shows the single-particle wave function for the ith valence nucleon, the explicit form of which is shown in Eq. (1). The subscript a_i in ϕ is the abbreviation of a set of the ith single-particle orbit, $a_i \equiv (n_i, l_i, j_i, m_i)$, while the vector $\boldsymbol{r}_i$ contains a set of the coordinates for the single-particle orbit, ($\boldsymbol{r}_i$, $\boldsymbol{\xi}_i$, $\boldsymbol{\eta}_i$). In Eq. (2), $\mathcal{A}$ and N mean the anti-symmetrization operator for two nucleons and the respective normalization constant, respectively.

The shell-model wave function in Eq. (2) does not have definite total spin J ($\boldsymbol{J} = \boldsymbol{j}_1 + \boldsymbol{j}_2$) but it is an eigenstate of the third component of the total spin of $J_z = j_{z1} + j_{z2}$. This wave function is used as a basis state for the configuration interaction (CI) calculations in the M-scheme codes (e.g., Ref. [17]). We omit the wave function of the inert core since its contribution disappears in the resultant expression owing to its orthogonality to the valence space.

The wave function of the di-nucleon ($2n$) cluster model is defined as

$$\Psi_c = N\mathcal{A}\left\{\chi_{LM}(\boldsymbol{R})\varphi_{SS_zTT_z}(\boldsymbol{\rho},\boldsymbol{\zeta})\right\} \tag{3}$$

with the core–2n relative wave function

$$\chi_{LM}(\boldsymbol{R}) = \hat{\chi}_L(R)\, Y_{LM}(\hat{\boldsymbol{R}}). \tag{4}$$

Here the core wave function is omitted again. $\hat{\chi}_L(R)$ and $Y_{LM}(\hat{\boldsymbol{R}})$ denote the radial and angular wave functions for the core–2n relative motion with the orbital spin L and its third component M. R and $\hat{\boldsymbol{R}}$ are the coordinates between the center of mass of the two nucleons and the core and its unit vector, respectively. $\varphi_{SS_zTT_z}(\boldsymbol{\rho}, \boldsymbol{\zeta})$ shows the internal wave function of the 2n cluster labeled by the intrinsic spin S (third component S_z) and the isospin T (third component T_z). The 2n internal wave function is given by the direct product of the spatial part of $\hat{\varphi}_\nu(\boldsymbol{\rho})$ and the spin–isospin part of $u_{SS_zTT_z}(\boldsymbol{\zeta})$ as

$$\varphi_{SS_zTT_z}(\boldsymbol{\rho}, \boldsymbol{\zeta}) = \hat{\varphi}_\nu(\boldsymbol{\rho}) \cdot u_{SS_zTT_z}(\boldsymbol{\zeta}), \tag{5}$$

which is a function of the relative coordinate of two nucleons, $\boldsymbol{\rho}$, and a set of the spin and isospin coordinates $\boldsymbol{\zeta}$. The spatial part of $\hat{\varphi}_\nu(\boldsymbol{\rho})$ is assumed to be a Gaussian function, $\hat{\varphi}_\nu(\boldsymbol{\rho}) = \hat{\varphi}_\nu(\rho) = (\nu/\pi)^{3/4}\, e^{-\frac{\nu}{2}\rho^2}$, which corresponds to the $(0s)^2$ configuration in the harmonic oscillator potential with a constant width ν.

The radial parts of the wave functions in the shell model $R_{nlj}(r)$ in Eq. (2) and the 2n-cluster model $\hat{\chi}_L(R)$ in Eq. (3) are solutions to the single-particle problem with a nuclear potential. In solving the single-particle problem, we employ the basis expansion technique with a tempered Gaussian basis [13]:

$$R_{nlj}(r) = \sum_i C_i^{(nlj)} \cdot r^l \exp\left(-\nu_i^{(nlj)} r^2\right) \tag{6}$$

$$\hat{\chi}_L(R) = \sum_j g_j^{(L)} \cdot R^L \exp\left(-\alpha_j^{(L)} R^2\right). \tag{7}$$

Here C_i and ν_i represent the variational parameters in the shell-model orbit for the ith basis, while g_j and α_j show those in the 2n-cluster model for the jth basis function.

2.2. *Computational condition for radial wave functions*

In the present analysis, we employ the harmonic oscillator (HO) wave function for both of the wave functions in the shell and cluster models to check the validity of our computational method, although the method can be applied to any type of wave function. The width parameter b_s ($\nu_s = 1/2b_s^2$) in the shell-model wave function is determined by $b_s = \sqrt{\hbar/m\omega}$ with $\hbar\omega = 41A_C^{-1/3}$, where A_C denotes the core mass number. Since the radial part of the HO wave function in Eq. (1) is independent of the spin and namely j, $R_{nlj}(r, \nu_s)$ can be replaced by $R_{nl}(r, \nu_s)$.

In the 2n-cluster model, the internal wave function of the 2n cluster shown in Eq. (5) is set to the singlet even state, corresponding to a di-neutron or di-proton cluster. In the present calculation, we do not solve the 2n wave function around a core nucleus but assume a simple Gaussian function of $\hat{\varphi}_\nu(\rho) \propto e^{-\frac{\nu}{2}\rho^2}$ with a 2b width parameter of b_{2n} and $\nu = 1/2b_{2n}^2$. The parameter ν is handled as a free parameter in the calculation of the shell–cluster overlap. As for the wave function for the core–2n relative motion, $\chi_{LM}(\boldsymbol{R})$ in Eq. (4), we do not solve the wave function but assume the simple HO wave function. The width parameter is set to $b_c = b_s/\sqrt{2}$ and $\alpha = 1/2b_c^2$, in which the factor of $\sqrt{2}$ originates from the mass number of 2n cluster. In the exact definition of the cluster wave function, this factor should be taken to the reduced mass number ($\sqrt{\mu}$) of core–2n but we use the approximation of the heavy core system ($\sqrt{\mu} \to \sqrt{2}$). The radial part of the HO wave function with α is expanded by the Gaussian bases as shown in Eq. (7).

In addition, we must consider the Wildermuth condition in the $2n$-cluster wave function to exclude the Pauli forbidden states from the core–$2n$ relative motion [26]. The forbidden states are evaluated by counting the total oscillator quanta N for the lowest allowed state. For instance, in the $^{16}\mathrm{O}+2n$ system, the relative motion of $\chi_{LM}(\boldsymbol{R})$ must satisfy the condition of $N \geq 4$, and hence $N < 3$ is forbidden, if we assume the filling configuration for the ^{16}O core, namely $(0s0p)$-closed configurations. If the core nucleus is not an LS-closed nucleus (^{16}O and ^{40}Ca) but a jj-closed one (^{28}Si, ^{32}S, and so on), the allowed state is not necessarily specified only by N. However, we assume that $\chi_{LM}(\boldsymbol{R})$ has the lowest allowed N with the lowest filling configuration of the core nucleus.

2.3. *Calculation of overlap integral by Fourier transformation*

We calculate the overlap integral of Eqs. (2) and (3), $\langle\Psi_s|\Psi_c\rangle$. In evaluating the overlap, we assume that the mass of the core nucleus is heavy, and the origin of the coordinates of the two nucleons $(\boldsymbol{r}_1, \boldsymbol{r}_2)$ and the core–$2n$ coordinate $(\boldsymbol{R})$ is the center of mass in the core nucleus. Even if we introduce the approximation of the heavy core, we must consider the coordinate rearrangement of $(\boldsymbol{r}_1, \boldsymbol{r}_2) \leftrightarrow (\boldsymbol{R}, \boldsymbol{\rho})$ in a normal way to calculate the overlap integral [13]. The introduction of the coordinate rearrangement is similar to the so-called hybrid calculation with T- and V-type bases in the core + n + n system [14].

Here we calculate the overlap integral on the basis of the Fourier transformation to avoid complexity in the coordinate rearrangement. In order to use the Fourier transformation, first we introduce the center-of-mass motion of the $2n$ cluster, $G(R) = (4\nu/\pi)^{3/4} e^{-2\nu R^2}$, and its reciprocal function $G^{-1}(R)$ for the cluster wave function as follows:

$$\begin{aligned}\Psi_c &= N\mathcal{A}\{\chi_{LM}(\boldsymbol{R})\varphi_{ST}(\boldsymbol{\rho},\boldsymbol{\zeta})\}\\ &= N\mathcal{A}\left\{\chi_{LM}(\boldsymbol{R})G^{-1}(R)\cdot G(R)\varphi_{ST}(\boldsymbol{\rho},\boldsymbol{\zeta})\right\}\\ &= N\mathcal{A}\{\tilde{\chi}_{LM}(\boldsymbol{R})\cdot G(R)\varphi_{ST}(\boldsymbol{\rho},\boldsymbol{\zeta})\}\end{aligned} \tag{8}$$

with $\tilde{\chi}_{LM}(\boldsymbol{R}) = \chi_{LM}(\boldsymbol{R})G^{-1}(R)$. Here the third components of the spin and isospin (S_z, T_z) in $\varphi_{SS_zTT_z}$ are omitted for simplicity. The spatial part in the product of $G\varphi_{ST}$ becomes

$$G(R)\varphi_{ST}(\boldsymbol{\rho},\boldsymbol{\zeta}) \propto G(R)\hat{\varphi}_\nu(\boldsymbol{\rho}) = N_1 e^{-\nu r_1^2}\cdot N_2 e^{-\nu r_2^2} \tag{9}$$

with the normalization constants of $N_1 = N_2 = (2\nu/\pi)^{3/4}$. The function of $N_i e^{-\nu r_i^2}$ $(i = 1, 2)$ represents the $0s$ orbits in the harmonic oscillator potential. If we introduce the Fourier representation for $\tilde{\chi}_{LM}(\boldsymbol{R})$,

$$\tilde{\chi}_{LM}(\boldsymbol{R}) = \frac{1}{\sqrt{(2\pi)^3}}\int d\boldsymbol{K}\tilde{X}_{LM}(\boldsymbol{K})e^{-i\boldsymbol{K}\cdot\boldsymbol{R}}, \tag{10}$$

and use the relation $\boldsymbol{R} = (\boldsymbol{r}_1 + \boldsymbol{r}_2)/2$, the $2n$-cluster wave function in Eq. (8) becomes

$$\Psi_c \propto \int d\boldsymbol{K}\tilde{X}_{LM}(\boldsymbol{K})\mathcal{A}\left\{e^{-i\frac{\boldsymbol{K}}{2}\cdot\boldsymbol{r}_1-\nu r_1^2}\cdot e^{-i\frac{\boldsymbol{K}}{2}\cdot\boldsymbol{r}_2-\nu r_2^2}\right\}. \tag{11}$$

Here the normalization constants are omitted. The overlap of the shell-model wave function in Eq. (2) and the cluster-model one in Eq. (3) with the Fourier representation in Eq. (11) can be calculated by employing the mathematical technique of the overlap B-matrix [7], which is composed of the overlaps of a set of single-particle orbits described by the single-particle coordinates, $\boldsymbol{r}_i$. Since all

of the wave functions in Eqs. (2) and (11) are written in terms of $(\boldsymbol{r}_1, \boldsymbol{r}_2)$, we can easily apply the B-matrix framework. Moreover, the momentum representation of $\hat{X}_{LM}(\boldsymbol{K})$ in the integrand in Eq. (11) can be expressed by the superposition of the tempered Gaussian functions, which are written in terms of the coefficients in the Gaussian expansion, g_j and α_j in Eq. (7), and the internal width of the $2n$ cluster, ν. Therefore, the momentum integration appearing in the overlap of $\langle\Psi_s|\Psi_c\rangle$ with the Fourier representation for Ψ_c in Eq. (11) can be done analytically, and the series of computational techniques can be easily extended to the calculation for four-nucleon systems.

After doing an analytic integration over the momentum $\boldsymbol{K}$, we obtain a simple expression

$$\begin{aligned}\langle\Psi_s|\Psi_c\rangle &= \langle\Psi_s(\boldsymbol{n},\boldsymbol{l},\boldsymbol{j},\boldsymbol{j}_z,\boldsymbol{\tau})|\Psi_c^{\nu}(LMSS_zTT_z)\rangle \\ &= F(LSS_zTT_z,\boldsymbol{l},\boldsymbol{j},\boldsymbol{j}_z,\boldsymbol{\tau})\cdot G^{\nu}(L,\boldsymbol{n},\boldsymbol{l},\boldsymbol{j}) \\ &\times \delta(M+S_z,\sum_{i=1}^{2} j_{zi}),\end{aligned} \tag{12}$$

where the bold symbols denote sets of quantum numbers of two nucleons, such as $\boldsymbol{n} = (n_1, n_2)$, $\boldsymbol{l} = (l_1, l_2)$. The $2n$-cluster-model wave function Ψ_c depends on the internal width parameters of the $2n$ cluster, ν, which is specified by the superscript in the first and second lines of Eq. (12). The Kronecker delta in the last line guarantees the conservation of the z-component of angular momentum.

In the second line of Eq. (12), the basic structure of the overlap integration is shown; specifically, the overlap integral is given by the direct product of the kinematic part F and the dynamical part G. F is determined by angular momentum algebra independent of the details of the radial wave functions, while G is calculated from two elements of the radial wave function: $R_{nlj}(r)$ in the shell model and $\hat{\chi}_L(R)$ in the cluster model. G contains the set of variational parameters shown in Eqs. (6) and (7): (C_i, ν_i) and (g_j, α_j). Thus, this part depends on the nuclear potential employed in solving the radial wave function.

The separable expression in Eq. (12) is useful to interpret the computational results for the overlap integrals in terms of the matching between the angular momentum scheme and the radial wave functions. This is an advantage arising from the Fourier transformation. The final expression becomes complicated if we employ the standard technique of coordinate rearrangement using the transformation of $(\boldsymbol{r}_1, \boldsymbol{r}_2) \leftrightarrow (\boldsymbol{R}, \boldsymbol{\rho})$ [13,14]. An explicit expression for the overlap integral in Eq. (12) is shown in the appendix in the case of the spin-singlet ($S = S_z = 0$), isospin-triplet ($T = |T_z| = 1$) pair of the two nucleons.

Although the Fourier transformation is useful in deriving the final expression of the overlap integral, there is a dangerous region in the integration over the momentum $\boldsymbol{K}$, where the Fourier transformation is impossible to define. In Eqs. (8), (10), and (11), we have introduced the Fourier representation for $\tilde{\chi}_{LM}(\boldsymbol{R})$, which is given by the product of the core–$2n$ relative wave function $\chi_{LM}(\boldsymbol{R})$ and $G^{-1}(R)$, being the inverse of the wave function of the center of mass in the $2n$ cluster. Since $G^{-1}(R) \sim e^{2\nu R^2}$ is a divergent function, the product of $\chi_{LM}(\boldsymbol{R})G^{-1}(R) \propto \hat{\chi}_L(R)G^{-1}(R)$ is not necessarily converged in the asymptotic region of $R \to \infty$.

Let us consider the divergent property in the $\boldsymbol{K}$ integration more clearly by showing an example of the harmonic oscillator (HO) wave function. If the radial part of the core–$2n$ relative wave function, $\hat{\chi}_L(R)$, is given by the pure HO wave function, $\hat{\chi}_L(R)$ has the functional form of (polynomial function) $\times\, e^{-\alpha R^2}$, where α corresponds to the width parameter of the employed HO potential. Thus, the

asymptotic behavior in $\hat{\chi}_L(R)G^{-1}(R)$ is determined by the Gaussian function of $e^{-(\alpha-2\nu)R^2}$. If the condition $\alpha > 2\nu$ is fulfilled, the momentum integration in the Fourier transformation in Eq. (10) is safely defined but the transformation is not well defined in the condition $\alpha \leq 2\nu$ because $\tilde{\chi}_{LM}(\boldsymbol{R}) \propto \hat{\chi}_L(R)G^{-1}(R)$ is not a spatially localized function.

The final expression for the overlap integral shown in Eq. (12) is analytically derived by assuming the condition $\alpha > 2\nu$. Therefore, we are to check the validity of the final expression of Eq. (12) in the region of $\alpha \leq 2\nu$, where the Fourier transformation is originally impossible to define, by comparison with the computational result using the coordinate rearrangement.

2.4. Configuration interaction

The expression of the overlap integral in Eq. (12) is calculated for the single configuration of the shell-model state Ψ_s but we can extend this single shell-model configuration to the superposition of the various configurations as follows:

$$\Psi_{s(a,b)} = \mathcal{NA}\left\{\phi_a^{(\tau_1)}(\boldsymbol{r}_1)\phi_b^{(\tau_2)}(\boldsymbol{r}_2)\right\}$$
$$\Psi_s^{\mathrm{CI}} = \sum_{a,b} C_{(a,b)}\Psi_{s(a,b)}, \tag{13}$$

where the subscripts a and b represent a set of the quantum numbers of the single-particle orbit shown in Eq. (1).

As explained in the previous section, the individual bases of $\Psi_{s(a,b)}$ do not have a definite total angular momentum but they have a good quantum number of the third component of the total spin of $J_z = j_{z1} + j_{z2}$. Coupling to the good quantum number of the total spin $\boldsymbol{J} = \boldsymbol{j}_1 + \boldsymbol{j}_2$ can be achieved by the superposition of the M-scheme basis [17]. Specifically, the total spin of the two nucleons is generated by superposing the different configurations with various j_{z1} and j_{z2} on the mixing amplitude $C_{(a,b)}$ in Eq. (13), and this mixing amplitude plays the role of the Clebsch–Gordan coefficients.

In recent studies, several computational codes for large-scale CI calculations have been developed. Here we use the KSHELL code to perform the CI calculation [17]; this code is easy to apply to various systems with jj-closed cores. The code is tuned for massively parallel computations by employing the thick-restart block Lanczos method [17]. The source of the computational program is publicly available, and the details of this code can be seen in Ref. [17]. By performing the CI calculations, we obtain the mixing amplitude $C_{(a,b)}$, which is used for calculating the overlap integral of the multi-CI-configuration Ψ_s^{CI} and the $2n$-cluster configuration Ψ_c according to the superposition in Eq. (13).

3. Results

3.1. Validity of Fourier transformation

The overlap integral is calculated for the system of the ^{16}O core plus two neutrons (n), where two neutrons occupy the $0d_{5/2}$ orbit with $j_{z1} = -j_{z2} = 5/2$. Here the shell model configuration is given by the direct product in Eq. (2). There are other combinations of j_{z1} and j_{z2}, such as $j_{z1} = -j_{z2} = 3/2$ and $1/2$, but the magnitude of the overlap is almost independent of the combination of j_{z1} and j_{z2}. The j_z dependence arises from the kinetic part F in Eq. (12) but the dependence is weak if the total spin

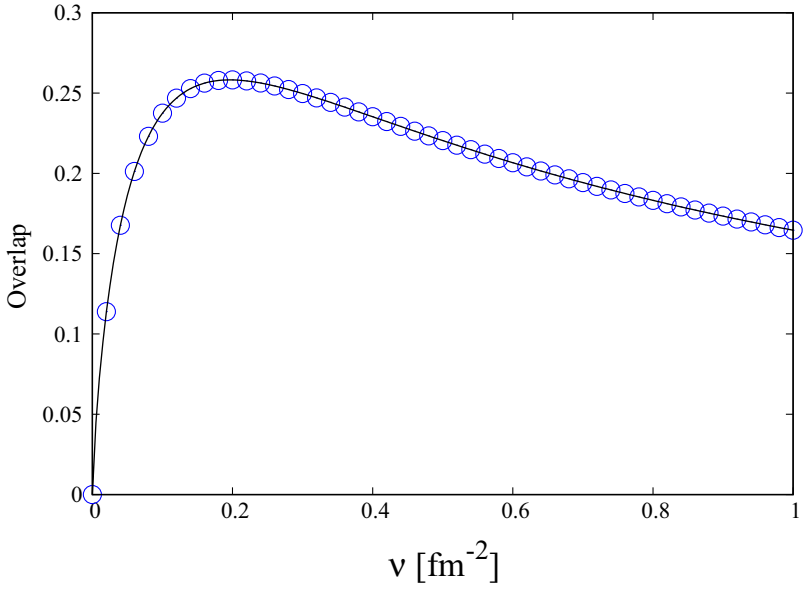

Fig. 1. Magnitude of the overlap integral calculated for the ^{16}O + n + n system. The abscissa and the ordinate represent the width parameter of the di-neutron cluster and the magnitude of the overlap, respectively. The solid curve denotes the result calculated from Fourier transformation, while the open circle shows the result from coordinate rearrangement.

of the individual single-particle orbits (j_1 and j_2) is fixed. Thus, we focus on the specific combination of $j_{z1} = -j_{z2} = 5/2$ to discuss the basic behavior of the overlap.

The orbital angular momentum is set to $L = M = 0$ for the $^{16}\mathrm{O} - 2n$ cluster wave function. The width parameter of the ^{16}O–2n cluster is fixed to $\alpha = 0.39$ fm^{-2}, which is evaluated from $\hbar\omega = 41 \cdot 16^{-1/3}$ MeV, while the internal parameter ν for the 2n cluster is varied. The ν dependence of the shell–cluster overlap integral between $^{16}\mathrm{O} + n + n$ and $^{16}\mathrm{O} + 2n$ is shown in Fig. 1. The solid curve shows the calculated result by the Fourier transformation, while the open circles represent that obtained from the calculation of the coordinate rearrangement.

In Fig. 1, we can see the increasing behavior from zero at $\nu = 0$ to the maximum peak at $\nu \sim 0.19$ fm^{-2}, and the magnitude decreases gradually as ν gets larger. Since we set $\alpha = 0.39$ fm^{-2} for the core–2n relative HO wave function, the position at $\nu \sim 0.19$ fm^{-2} satisfies $\alpha = 2\nu$, which corresponds to the boundary of the definition of the Fourier transformation discussed in Sect. 2.3. In the region of $\nu < 0.19$ fm^{-2} ($\alpha - 2\nu > 0$), the function of $\tilde{\chi}_{LM}(\boldsymbol{R}) \propto \hat{\chi}_L(\boldsymbol{R})G^{-1}(R)$ becomes a damping function in $R \to \infty$, while it is a non-converged function in the region of $\nu \geq 0.19$ fm^{-2} ($\alpha - 2\nu \leq 0$), and hence the Fourier transformation in Eq. (11) cannot be defined. In spite of that, the result of the Fourier transformation (solid curve) gives the same result as that obtained from the calculation of the coordinate rearrangement (open circles). This agreement means that the Fourier transformation can be applied to any range of internal 2n-widths independent of the width parameter of the core–2n relative wave function.

3.2. Orbit dependence of overlap integral

We investigate the relationship between the overlap integral and the shell-model orbits. To see the orbit dependence in the shell–cluster overlap, systems composed of two neutrons plus LS-closed cores, ^{16}O and ^{40}Ca, are considered. In the following results, the width parameter of the 2n cluster is fixed to be $\nu = 0.082$ fm^{-2}. This width parameter reproduces the root-mean-squared radius of a

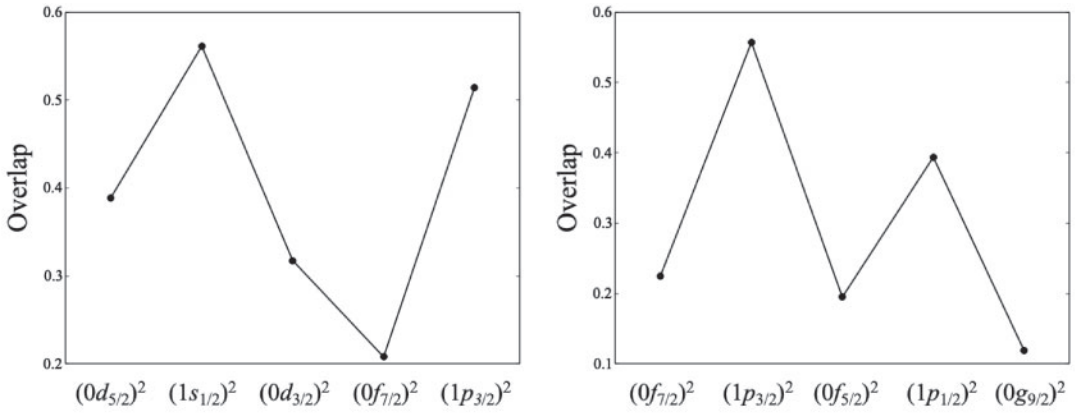

Fig. 2. Left: magnitude of the overlap in the ^{16}O core plus two neutrons. The ordinate shows the magnitude of the overlap, while the shell-model orbits occupied by two neutrons are shown in the abscissa. Right: Same as the left panel except for a ^{40}Ca core.

deuteron, $\sqrt{\langle r^2 \rangle} \sim 2.1$ fm. In Fig. 2, the magnitudes of the overlap integrals in $^{16}\mathrm{O} + n + n$ and $^{40}\mathrm{Ca} + n + n$ are shown in the left and right panels, respectively. In both panels, the ordinate means the magnitude of the overlap, while the shell-model configurations for the two neutrons are labeled in the abscissa. Here the relative spin of core–$2n$ is set to $L = M = 0$, and $(S, T) = (0, 1)$ is assumed for the spin–isospin configuration in the $2n$ cluster. In the shell-model wave function, two neutrons form the zero pair as $\boldsymbol{J} = \boldsymbol{j}_1 + \boldsymbol{j}_2 = \boldsymbol{0}$, which is given by the two-neutron wave functions

$$\Psi_s^{J=0} = \frac{1}{\sqrt{1+\delta_{j_1,j_2}}} \frac{1}{\sqrt{2!}} \mathcal{A} \left[\phi_{j_1}^{(n)}(\boldsymbol{r}_1) \otimes \phi_{j_2}^{(n)}(\boldsymbol{r}_2) \right]_{J=J_z=0}, \tag{14}$$

where the core wave function is omitted. When two neutrons occupy a common shell-model orbit, an extra factor of $1/\sqrt{1+\delta_{j_1,j_2}}$ is needed in addition to the normalization constant for the anti-symmetrization $1/\sqrt{2!}$.

In the two panels of Fig. 2, we can see characteristic peak structures at the specific orbits: s and p orbits with the ^{16}O core (left) and p orbits with the ^{40}Ca core (right). The magnitude of the overlap is enhanced when the shell-model orbits have low orbital angular momenta, such as $l = 0$ and 1, in both of the core nuclei but it decreases in orbits with higher orbital angular momenta, such as the f and g orbits. This tendency is reasonable because the $2n$-cluster configuration is set to the s-wave state: $L = M = 0$ for the core–$2n$ relative motion and $S = 0$ for the $2n$ cluster. Shell-model orbits with lower orbital spins have a large overlap with the spinless state of the $2n$ cluster.

It is very interesting to decompose the overlap integral into two parts, the kinematic part F and the dynamical part G, according to Eq. (12). F and G are given by the angular momentum algebra and the spatial distribution of the radial wave functions, respectively. The results of the decomposition are shown in Fig. 3, in which the left and right panels show the results of $^{18}\mathrm{O} = {}^{16}\mathrm{O} + n + n$ and $^{42}\mathrm{Ca} = {}^{40}\mathrm{Ca} + n + n$, respectively. In both panels, the solid lines represent the magnitudes of the overlap integrals, which are the same as the lines in Fig. 2, while the dotted and dashed lines show the kinematic part F and the dynamical part G, respectively.

When we focus on the dashed line (dynamical part G) in the left panel, its magnitude for $(1s_{1/2})^2$ is the lowest of all orbits. However, the amplitude in the dotted line (kinematic part F) is the highest, and this highest value of F leads to the maximum of the final overlap shown by the solid line. Thus, the enhancement at $(1s_{1/2})^2$ in ^{18}O is due to the predominance of the kinematic part F. On the other

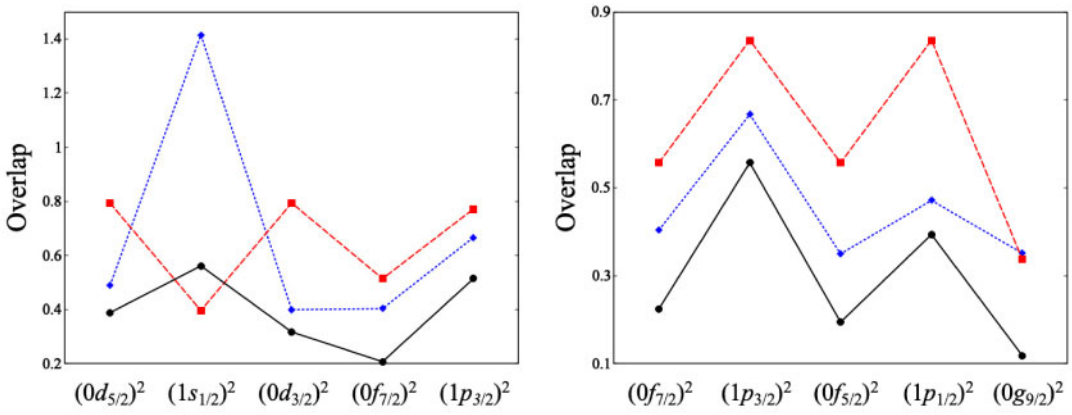

Fig. 3. Decomposition of the overlap integral into kinematic (F) and dynamical (G) parts. The left and right panels show the result of ^{16}O + n + n and ^{40}Ca + n + n, respectively. In both panels, the ordinate shows the magnitude of the overlap, F and G, while the abscissa represents the shell-model configuration for two valence neutrons. F and G are plotted by dotted and dashed lines, respectively. The solid lines show the overlaps and are the same as the solid lines in Fig. 2.

hand, in the $(1p_{3/2})^2$ orbit shown by the right-most point in the left panel, both of the F and G parts coherently enhance the overlap, which is shown as the solid line.

The tendency that is confirmed in the p-wave orbit in ^{18}O can also be seen in the result of ^{42}Ca in the right panel. The overlap in ^{42}Ca is enhanced at the $(1p_{3/2})^2$ and $(1p_{1/2})^2$ orbits, and these enhancements originate from the coherent enhancement of the kinematic part F (dotted line) and the dynamical part G (dashed line).

In marked contrast to the results for the s and p orbits, the overlap integral is suppressed in the shell-model orbit with higher orbital angular momentum, such as the f and g orbits. In these higher orbits, the reduction of the overlap is due to simultaneous suppression in both F and G. Since we assume a spinless structure for the $2n$ cluster ($L = S = 0$), the overlap with the shell-model configuration with the higher orbital spin is considered to be suppressed.

3.3. *Systematic analysis of core + n + n systems*

We extend the analysis of the overlap integral to various systems with jj-closed cores: ^{16}O, ^{28}Si, ^{32}S, ^{40}Ca, ^{56}Ni, ^{56}Ge, and ^{76}Sr. In Fig. 4, we show the systematics of the overlap integral for the jj-closed core-plus-two-neutrons systems. The dotted line shows the overlap calculated from the neutron pair with $J_z = j_{z1} + j_{z2} = 0$ in the shell-model orbit, while the solid line denotes the overlap with the spin-zero pair of the shell-model orbits, $\boldsymbol{J} = \boldsymbol{j}_1 + \boldsymbol{j}_2 = \boldsymbol{0}$. In the $J_z = 0$ configurations, we consider only combinations of the maximum $|j_{z1}|$ and $|j_{z2}|$, such as $j_{z1} = -j_{z2} = 5/2$ in $(0d_{5/2})^2$, because the overlap does not strongly depend on the combination of j_{z1} and j_{z2}. Here the $J = 0$ states are normalized to unity by introducing the extra factor of $1/\sqrt{1+\delta_{j_1,j_2}}$ as pointed out in Eq. (14).

In the $J_z = 0$ configuration (dotted line), the total spin of two neutrons in the shell-model orbit is not a good quantum number, and hence the difference between the dotted line ($J_z = 0$) and the solid line ($J = 0$) corresponds to the effect of the angular momentum projection. The angular momentum projection from $J_z = 0$ to $J = 0$ enhances the magnitude of the overlap integral except for $(1s_{1/2})^2$ with ^{28}Si and $(1p_{1/2})^2$ with ^{76}Sr, in which the $J_z = 0$ pair is equivalent to the $J = 0$ pair due to the Pauli principle. The enhancement in the shell–cluster overlap projected to $\boldsymbol{J} = 0$ (solid line) is

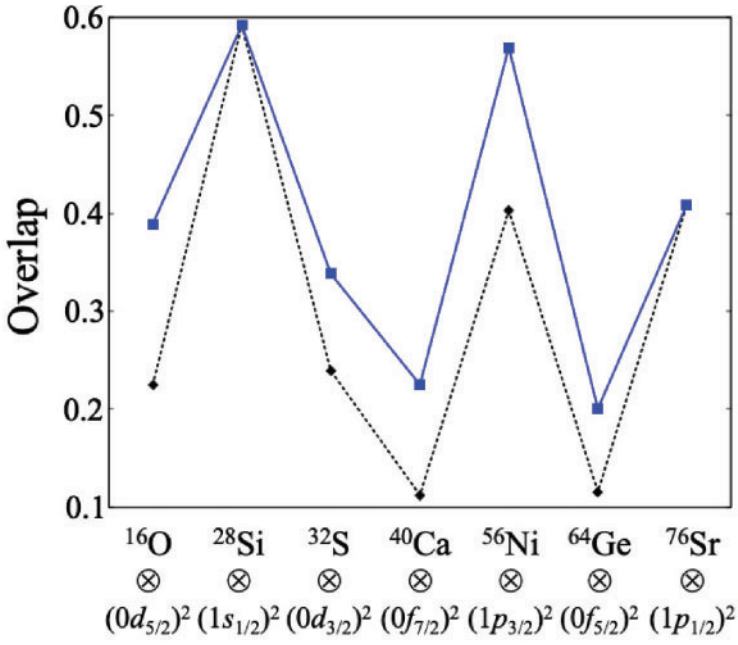

Fig. 4. Systematics of the overlap amplitude calculated with various cores. In the abscissa, the core nucleus and the shell-model orbit occupied by two neutrons are specified. The dotted line shows the results calculated with the shell-model configuration of $J_z = 0$, while the solid one shows the results of the $\boldsymbol{J} = 0$ pair configuration.

natural because the $2n$-cluster wave function has a total spin of zero with $L = S = 0$ in the present condition.

In Fig. 4, prominent enhancements appear at the configurations of $(1s_{1/2})^2$ with ^{28}Si and $(1p)^2$ with ^{56}Ni and ^{76}Sr. As we have confirmed in Fig. 2, the magnitude of the overlap with the core of ^{16}O and ^{40}Ca is increased when two neutrons occupy shell-model orbits with lower orbital angular momenta, such as $l = 0$ and 1. Similar enhancements also occur in the systematic calculations with various jj-closed cores; specifically, the overlaps increase when two valence neutrons can occupy the s or p orbits due to full occupation of the low-lying orbits below the s or p orbits by the core nucleus.

Since the magnitude of the overlap integral depends on the width parameter of the $2n$ cluster, ν, we should check the width dependence in the systematic calculation of the overlap. The ν dependence of the shell–cluster overlap is shown in Fig. 5. In this figure, the dotted line shows the overlap calculated with the $2n$-width of $\nu = 0.082$ fm^{-2}, while the solid line shows the overlap with the reduced $2n$-width, $\nu = 0.26$ fm^{-2}. The former width is fixed to reproduce the root-mean-squared radius of the deuteron ($\sim$ 2.1 fm), while the latter one is frequently used in the α-cluster model [5–7].

The $2n$-width based on the deuteron (dotted line) enhances the overlap in the heavier cores of ^{56}Ni, ^{64}Ge, and ^{76}Sr but the width determined from the size of the α cluster gives a large overlap in lighter cores such as ^{16}O, ^{28}Si, and ^{32}S. The difference using these widths is the smallest in the ^{40}Ca core. As can be seen in Fig. 5, the peak–valley structure is invariant in the variation of the width parameter for the $2n$ cluster, although the magnitude of the overlap slightly depends on the setting of the width parameter. We can clearly confirm the enhancements in the overlap due to the occupation of the s and p orbits by valence two neutrons even if the width parameters are varied over a reasonable range.

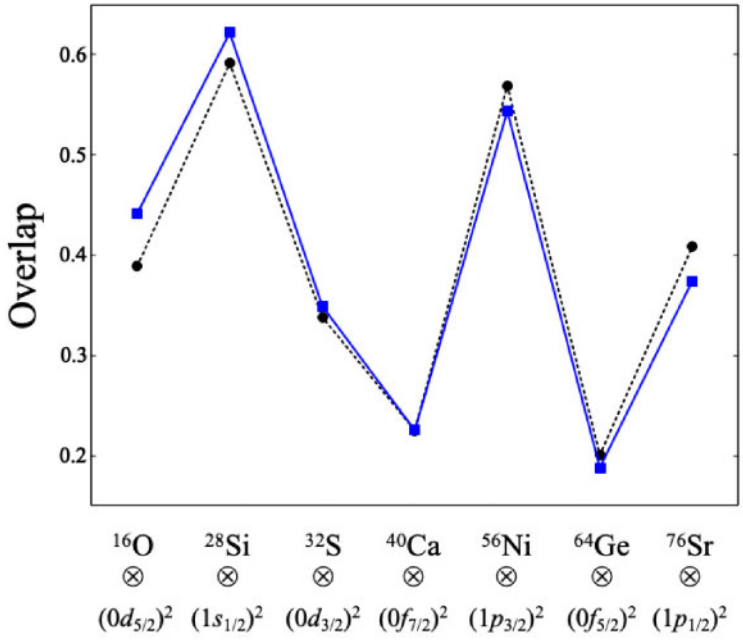

Fig. 5. Systematics of the overlap in core + n + n systems with different width parameters for the $2n$ cluster (ν). The solid line shows the overlap calculated by the width parameter of $\nu = 0.26$ fm^{-2}, while the dotted one represents the result with the parameter of $\nu = 0.082$ fm^{-2}. Both lines are the results of the $\boldsymbol{J} = 0$ pair of two neutrons, and the dotted line is the same as the solid line shown in Fig. 4.

Table 1. Interactions and model spaces used in the configuration interaction calculation. All of the interactions are equipped with the computational code of KSHELL [17].

Core	Interaction	Model space
^{16}O, ^{28}Si, ^{32}S	SDPF-M [27]	$1s0d$, $0f_{7/2}$, and $1p_{3/2}$
^{40}Ca, ^{56}Ni	GXPF1A [28]	$1p0f$
^{64}Ge, ^{76}Sr	JUN45 [29]	$1p$, $0f_{5/2}$, and $0g_{9/2}$

The result in Fig. 4 is obtained by assuming naive shell-model configurations for the valence two neutrons, i.e. the occupation of the lowest orbit around the core. In realistic nuclei, however, there must be an effect from the configuration interaction (CI), and we should check the CI effect on the systematics in the overlap integral. In order to see the CI effect on the shell–cluster overlap, we have performed a CI calculation employing the computational code of KSHELL [17]. The interactions and model spaces used are listed in Table 1. Here we use the interactions of SDPF-M [27], GXPF1A [28], and JUN45 [29].

For example, the SDPF-M interaction [27] is applied to systems with cores of ^{16}O, ^{28}Si, and ^{32}S plus two valence neutrons, and the CI calculations are performed for the two neutrons. The full configuration is considered in the calculation of ^{16}O + n + n, while the model space is truncated for the cores in the calculations of ^{28}Si + n + n and ^{32}S + n + n; specifically, 12 nucleons in ^{28}Si and 16 nucleons in ^{32}S around ^{16}O are frozen in the $(0d_{5/2})^{12}$ and $(0d_{5/2})^{12}(1s_{1/2})^4$ configurations, respectively. The truncations are applied in the same manner for the other cases except for the ^{40}Ca + n + n case, and all nucleons contained in the individual cores around ^{40}Ca are fixed at the lowest shell-model configurations: $(0f_{7/2})^{16}$ in ^{56}Ni, $(0f_{7/2})^{16}(1p_{3/2})^8$ in ^{64}Ge, and $(0f_{7/2})^{16}(1p_{3/2})^8(0f_{5/2})^{12}$ in ^{76}Sr.

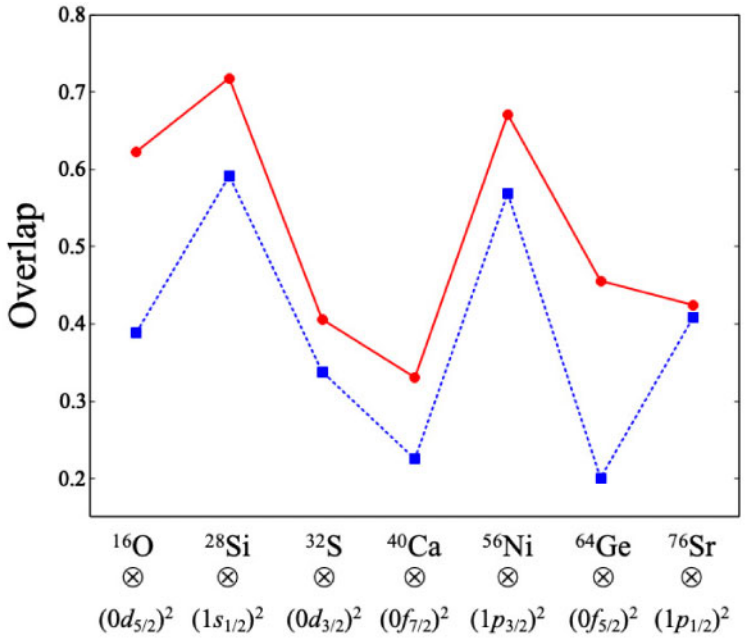

Fig. 6. Comparison of overlaps with and without configuration interaction (CI). The dotted line shows the results without CI, while the results with CI are plotted by the solid line. The core nucleus and the lowest orbit occupied by two neutrons are shown in the abscissa. The dotted line shows the result of the $\boldsymbol{J} = 0$ pair for a two-neutron configuration, which is the same as the solid line in Fig. 4 and the dotted one in Fig. 5

A comparison of the results with and without the CI effect is shown in Fig. 6. In this figure, the dotted line shows the overlap without CI, which should be called the "uncorrelated pair of nucleons" in the naive shell-model picture, while the solid line describes the "correlated pair of two nucleons" taking into account the CI effect summarized in Table 1. The result with CI (solid line) is more enhanced than that without CI (dotted line) by a factor of about 1.3–3, except for the ^{76}Sr core. The formation of a $2n$ cluster with a spatially localized configuration requires a mixture of higher orbital spin due to the uncertainty relation of $\Delta L \cdot \Delta\theta \sim \hbar$ with the fluctuation of the orbital spin ΔL and the opening angle of correlated pairs of nucleons $\Delta\theta$ [30]. Since the CI effect generates a mixture of excited orbits with higher orbital spins, the enhancement of the overlap with the $2n$ cluster by the CI effect is considered to be a natural result.

The small enhancement at the ^{76}Sr core is due to the insufficiency of the model space. In the present CI calculation of ^{76}Sr + n + n, the interaction of JUN45 is employed as shown in Table 1 but the active configuration in the CI calculation for two neutrons is limited to $(0g_{9/2})^2$ because all $1p0f$ orbits are exactly occupied by the ^{76}Sr core and two neutrons. Furthermore, the coupling of the $1p_{1/2}$ and $0g_{9/2}$ orbits is small due to the large difference in the orbital angular momentum. These are the reasons why the CI effect is minor in the present calculation for ^{76}Sr + n + n.

Although a spherical shape is assumed for the ^{76}Sr core in the present CI calculation, the ^{76}Sr nucleus is a strongly deformed nucleus with a prolate shape, which can be described by a large-scale CI calculation based on the active model space of the $1p0f$ and $0g1d$ shells built on the ^{56}Ni core [31]. The analysis in Ref. [31] showed that the quasi-SU(3) coupling of the $0g_{9/2}$ and $1d_{5/2}$ orbits plays an important role in reproducing the large collectivity in ^{76}Sr. Therefore, the deformation effect in ^{76}Sr should be taken into account in a realistic calculation of the shell–cluster overlap integrals.

From a comparison of the solid line with the dotted one in Fig. 6, we can understand that the CI effect does not change the peak–valley structure, which was originally generated in the calculation without the CI effect, too much. Specifically, the feature of the enhancement (suppression) at the 1s and 1p (0f and 0g) orbits is unchanged even if the CI effect is taken into account. Roughly speaking, the CI effect enhances the magnitude of the overlap but its amount is almost constant over all of the core systems except for the ^{76}Sr core. Thus, the peak structure without CI survives after switching on the CI effect, and we can trace the original peak structure, which appears in the naive shell-model configuration, from the CI solutions.

4. Summary

In summary, we have formulated a computational technique to calculate the overlap integral of the shell model and the cluster model by showing examples of the core plus valence two nucleons. The formulation is achieved by introducing the Gaussian expansion method (GEM) [13,15,16] and the Fourier transformation (FT) in the basic expression of the overlap integral. In the computational method of GEM + FT, we can apply the standard technique of the B-matrix to the calculation of the shell–cluster overlap integral, and hence an extension to more complicated problems is also possible in a straightforward manner. Furthermore, the final expression of the overlap integral derived from the Fourier transformation becomes simple; it is given by the direct product of the kinematic part and the dynamical part. The former is calculated from the Clebsch–Gordan coefficients in the angular momentum algebra, while the latter is defined by the integration of the radial wave function.

It is instructive to emphasize the advantages of the GEM + FT method in practical applications. In this method, we can use an arbitrary functional form for the relative wave function between the core and the valence particles (core–nucleons and core–cluster), which is prepared by the superposition of Gaussian bases. Flexible treatment of the relative wave functions is quite important in application to realistic systems in extreme conditions, such as weakly bound resonant or heavy-core-plus-α systems. In the former case, the wave functions are spatially extended, while the wave function reveals highly oscillating behavior in the latter case. GEM + FT can handle both of these extreme conditions in a simple mathematical formula, and this is superior to the traditional computational method, the Talmi–Moshinsky transformation [18,19]. In the GEM + FT method, the internal wave function of the cluster is assumed to be the 0s wave function in the harmonic oscillator potential but this assumption is expected to be valid at least for the ^{3}H, ^{3}He, and α clusters according to previous studies using cluster models [5–7].

In order to check the validity of the computational method of the shell–cluster overlap using GEM + FT, we apply the method to the system of ^{16}O plus two neutrons. Although the Fourier transformation is not necessarily defined in the whole parameter space, composed of the width parameters for the 2n internal motion and the core–2n relative one, we have demonstrated that the computation by the Fourier transformation gives the same result as that using the coordinate rearrangement in the whole parameter space. This result demonstrates the validity of our framework based on the Fourier transformation, and hence we can safely apply this method to general systems.

We have calculated the shell–cluster overlap in systems with LS-closed cores, ^{16}O and ^{40}Ca nuclei, plus two neutrons based on the harmonic oscillator (HO) wave function. As for the 2n-cluster wave functions, the Wildermuth condition is considered in the core–2n HO wave function. We have found that the shell–cluster overlap integral is prominently enhanced if two neutrons occupy shell-model orbits with the lower orbital angular momenta, such as the 1s and 1p orbits.

The total magnitude of the overlap is decomposed into the kinematic part and the dynamical part to see the origin of the enhancement in these orbits with lower angular momenta. The enhancement in the $1s$ orbit is mainly caused by the enhancement in the kinematic part, while both of the contributions increase in the overlap with the $1p$ orbit. As the orbital angular momentum in the shell-model orbit is higher, such as in the $0f$ and $0g$ orbits, both of the contributions decrease, which leads to the suppression of the total magnitude of the overlap. These results are quite valid because we assume a spinless structure for the $2n$ cluster, and shell-model orbits with lower orbital spins must have a large overlap with a spinless $2n$ cluster.

The tendency for the enhanced overlap in the s and p orbits can also be seen in the systematic calculation by varying the core nuclei. Here we have assumed jj-closed cores, and the overlap integral of the shell-model configuration (core + n + n) and the cluster-model one (core + $2n$) is evaluated. As confirmed in the calculations of ^{16}O + n + n and ^{40}Ca + n + n, the magnitude of the overlap integrals is enhanced at the occupation of the $1s_{1/2}$, $1p_{3/2}$, and $1p_{1/2}$ orbits, which correspond to the ^{28}Si, ^{56}Ni, and ^{76}Sr cores, respectively. We have investigated the effect of the total spin projection for the shell-model configuration by comparing the $J_z = 0$ pair with the $\boldsymbol{J} = 0$ pair. The spin projection for the shell-model configuration enhances the magnitude of the shell–cluster overlap but the effect of the projection is not so important for the peak structure in the shell–cluster overlap.

Finally, a calculation of the configuration interaction (CI) is performed for the valence two neutrons, and the CI effect is taken into account in the evaluation of the overlap integrals. The formulation of our overlap integrals is based on the M-scheme in the CI calculation, and it can be directly combined with the M-scheme CI calculation. In the present analysis, we have employed the computational code of KSHELL [17].

The CI effect increases the magnitudes of the overlap integrals and the formation probability of the $2n$ cluster is enhanced by the CI effect. This is a reasonable consequence of the uncertainty relation of $\Delta L \cdot \Delta\theta \sim \hbar$ for the fluctuation of the orbital angular momentum ΔL and the opening angle of the two nucleons $\Delta\theta$ measured from the center of the core nucleus. Since the CI effect takes into account the large fluctuation in ΔL by superposing the shell-model orbits with higher L, $\Delta\theta$ is reduced after including the CI effect. A similar enhancement to it has already been pointed out in the study of the di-neutron correlation on the basis of the Hartree–Fock–Bogoliubov calculation in medium-heavy nuclei [30].

Although the CI effect increases the magnitude of the overlap, its amount is almost constant in all of the systems with the jj-closed core. Therefore, the regularity of the enhanced overlap due to the occupation of the $1s$ and $1p$ orbits survives after including the CI effect. This consequence is expected to be valid, at least for spherical core systems, and we can expect enhancement of the overlap integrals on the basis of the naive shell-model configuration in such spherical systems. Moreover, there is a possibility that the regularity relevant to the $1s$ and $1p$ orbits can be generalized to other cluster systems, deuteron, tritium, ^{3}He, and α, because all of these clusters are constructed from a direct product of the $0s$ single-particle orbit, which is similar to the $2n$ clusters treated here. A systematic analysis of the shell–cluster overlap with these $0s$ clusters is now in progress.

Acknowledgements

We would like to thank Mrs N. Nishida, Mr M. Matsushita, R. Ikegawa, H. Yamada, and all the members of the Quantum Many-Body Physics Laboratory at Kansai University for their useful discussions and kind support. One of the authors (M.I.) thanks Profs H. G. Masui at the Kitami Institute of Technology; T. Yamada and Y. Funaki at Kanto-Gakuin University; and H. Otsu, J. Tanaka, S. Abe, and S. Koyama at RIKEN for

their valuable discussions, useful comments, and encouragement. N.S. acknowledges valuable support by the "Program for Promoting Researches on the Supercomputer Fugaku", MEXT, Japan. This work is supported by a Grant-in-Aid for Scientific Research, KAKENHI, No. JP21K03561.

A. Appendix

In this appendix, we show the expression of the overlap integral of the shell-model and cluster-model wave functions in core-plus-two-neutrons systems.

A.1. Definition of wave functions

The shell-model wave function of the two valence neutrons, which move around the heavy core, is written in symbolic form as follows:

$$\Psi_s = N_s \mathcal{A}\{\phi_1(\boldsymbol{r}_1, \boldsymbol{\sigma}_1)\phi_2(\boldsymbol{r}_2, \boldsymbol{\sigma}_2)\}, \tag{A.1}$$

with the normalization constant of $N_s = 1/\sqrt{2!}$. $\phi_i(\boldsymbol{r}_i, \boldsymbol{\sigma}_i)$ denotes the single-particle wave function for the ith neutron with spatial ($\boldsymbol{r}_i$) and spin ($\boldsymbol{\sigma}_i$) coordinates. Here the isospin part is omitted for simplicity. The subscript i in ϕ_i represents a set of quantum numbers: the radial node number n, the orbital spin l, the total spin j, its third component j_z for the ith neutron, and hence $i \equiv (n_i, l_i, j_i, j_{z_i})$. In Eq. (A.1), the core part in the wave function is omitted, and we consider only the two neutron degrees of freedom. Since the single-particle wave functions of the two valence neutrons and those in the core wave function are orthogonal to each other, the core part vanishes in the final expression of the overlap integral.

The explicit form of the single-particle wave function is given by

$$\phi_{nljj_z\tau}(\boldsymbol{r}, \boldsymbol{\sigma}) = \sum_{m\nu} \langle\, l\ m\ \frac{1}{2}\ \nu \mid j\ j_z\ \rangle R_{nlj}(r) Y_{lm}(\hat{\boldsymbol{r}}) v_{1/2\nu}(\boldsymbol{\sigma}), \tag{A.2}$$

which is composed of the radial function $R_{nlj}(r)$, the spherical harmonics $Y_{lm}(\hat{\boldsymbol{r}})$ with the third component of the orbital spin m, and the spin function $v_{1/2\nu}(\boldsymbol{\sigma})$ with the third component of the nucleon spin ν. The bracket shows the Clebsch–Gordan coefficient to generate the good quantum number of the total spin j.

The radial wave function of R_{nlj} in the individual single-particle wave functions is expanded by the tempered Gaussian function as

$$R_{nlj}(r) = \sum_a C_a^{(nlj)} \cdot r^l \exp(-\nu_a^{(nlj)} \cdot r^2), \tag{A.3}$$

where $C_a^{(nlj)}$ and $\nu_a^{(nlj)}$ mean the expansion coefficient and the width parameters for the ath basis in the quantum state described by n, l, and j.

On the other hand, the wave function of the cluster model is set to

$$\Psi_c = N_c \mathcal{A}\left\{\chi_{LM}(\boldsymbol{R}) \cdot \varphi^{\nu}(\boldsymbol{\rho}, \boldsymbol{\sigma}_1, \boldsymbol{\sigma}_2)\right\} \tag{A.4}$$

with a normalization constant of $N_c = 1/\sqrt{2!}$. Again, the core wave function and the isospin function for the two neutrons are dropped for simplicity. $\chi_{LM}(\boldsymbol{R})$ represents the core–2n relative wave function, which is a direct product of the radial part $\hat{\chi}_L(R)$ and the angular part $Y_{LM}(\hat{\boldsymbol{R}})$:

$$\chi_{LM}(\boldsymbol{R}) = \hat{\chi}_L(R) Y_{LM}(\hat{\boldsymbol{R}}). \tag{A.5}$$

Here $\boldsymbol{R}$ describes the core–$2n$ relative coordinate with the radial part R and the angular part $\hat{\boldsymbol{R}}$. The radial part of the relative wave function is expanded by the tempered Gaussian, which is similar to the treatment in Eq. (A.3),

$$\hat{\chi}_L(R) = \sum_j g_j^{(L)} \cdot R^L \exp\left(-\alpha_j^{(L)} R^2\right), \tag{A.6}$$

which contains the expansion parameters of $g_j^{(L)}$ and $\alpha_j^{(L)}$.

In Eq. (A.4), $\varphi^\nu(\boldsymbol{\rho}, \boldsymbol{\sigma}_1, \boldsymbol{\sigma}_2)$ shows the internal wave function of the $2n$ cluster depending on the n–n relative coordinate $\boldsymbol{\rho}$ and the spin coordinate $(\boldsymbol{\sigma}_1, \boldsymbol{\sigma}_2)$. The superscript ν denotes the width parameter for the radial wave function. The explicit expression of the $2n$ internal wave function is given by

$$\begin{aligned}\varphi^\nu(\boldsymbol{\rho}, \boldsymbol{\sigma}_1, \boldsymbol{\sigma}_2) &= \hat{\varphi}^\nu(\boldsymbol{\rho}) \left[v_{\frac{1}{2}}(\boldsymbol{\sigma}_1) \otimes v_{\frac{1}{2}}(\boldsymbol{\sigma}_2) \right]_{S=0, S_z=0} \\ &= \hat{\varphi}^\nu(\boldsymbol{\rho}) \sum_{\nu_1', \nu_2'} \langle \frac{1}{2} \nu_1' \frac{1}{2} \nu_2' | 00 \rangle v_{\frac{1}{2}\nu_1'}(\boldsymbol{\sigma}_1) v_{\frac{1}{2}\nu_2'}(\boldsymbol{\sigma}_2),\end{aligned} \tag{A.7}$$

which contains the radial function of

$$\hat{\varphi}^\nu(\boldsymbol{\rho}) = \left(\frac{2\nu_r}{\pi}\right)^{\frac{3}{4}} e^{-\nu_r \rho^2} \tag{A.8}$$

with the width parameter of $\nu_r = \nu/2$. The internal function in Eq. (A.7) with Eq. (A.8) describes the $2n$ cluster with the spin singlet pair ($S = S_z = 0$), corresponding to the $(0s_{1/2})^2$ configuration in a simple harmonic oscillator potential with a width of ν.

A.2. Shell–cluster overlap by Fourier transformation

We calculate the shell–cluster overlap of $\langle \Psi_s | \Psi_c \rangle$ using the definitions of the wave function explained before. In the calculation of the overlap, first we introduce the wave function for the center-of-mass motion of the $2n$ cluster, $G(R) = (4\nu/\pi)^{3/4} e^{-2\nu R^2}$, and its inverse $G^{-1}(R)$ for the cluster wave function as

$$\begin{aligned}\Psi_c &= N_c \mathcal{A} \left\{ \chi_{LM}(\boldsymbol{R}) \varphi^\nu(\boldsymbol{\rho}, \boldsymbol{\sigma_1}, \boldsymbol{\sigma_2}) \right\} \\ &= N_c \mathcal{A} \left\{ \chi_{LM}(\boldsymbol{R}) G^{-1}(R) \cdot G(R) \varphi^\nu(\boldsymbol{\rho}, \boldsymbol{\sigma_1}, \boldsymbol{\sigma_2}) \right\} \\ &= N_c \mathcal{A} \left\{ \tilde{\chi}_{LM}(\boldsymbol{R}) \cdot G(R) \varphi^\nu(\boldsymbol{\rho}, \boldsymbol{\sigma_1}, \boldsymbol{\sigma_2}) \right\}\end{aligned} \tag{A.9}$$

with $\tilde{\chi}_{LM}(\boldsymbol{R}) = \chi_{LM}(\boldsymbol{R}) G^{-1}(R)$. The spatial part in the product of $G\varphi^\nu$ becomes the direct product of the single-particle wave function in the $0s$ orbit.

Second, we introduce the Fourier representation for $\tilde{\chi}_{LM}(\boldsymbol{R})$:

$$\tilde{\chi}_{LM}(\boldsymbol{R}) = \frac{1}{\sqrt{(2\pi)^3}} \int d\boldsymbol{K} \tilde{X}_{LM}(\boldsymbol{K}) e^{-i\boldsymbol{K}\cdot\boldsymbol{R}}. \tag{A.10}$$

The integrand $\tilde{X}_{LM}(\boldsymbol{K})$ can be expressed by the internal width of the $2n$ cluster, ν, and the expansion coefficients, g_j and α_j, in the relative wave function $\chi_{LM}(\boldsymbol{R})$ in Eq. (A.6). After simple calculations with the relation in the coordinate of $\boldsymbol{R} = (\boldsymbol{r}_1 + \boldsymbol{r}_2)/2$, we can obtain the following expression for the overlap:

$$\langle \Psi_s | \Psi_c \rangle = \langle \Psi_s(\boldsymbol{n}, \boldsymbol{l}, \boldsymbol{j}, \boldsymbol{j_z}) | \Psi_c^\nu(LM) \rangle$$

$$= F(L,\boldsymbol{l},\boldsymbol{j},\boldsymbol{j_z}) \cdot G^{\nu}(L,\boldsymbol{n},\boldsymbol{l},\boldsymbol{j}) \cdot \delta(M,\sum_{i=1}^{2} j_{zi}), \tag{A.11}$$

which has a simple product of F and G^{ν}. In this expression, the bold symbols represent the set of quantum numbers for the two neutrons, such as $\boldsymbol{n} = (n_1, n_2)$, $\boldsymbol{l} = (l_1, l_2)$, and so on, while δ in the second line shows a Kronecker delta to guarantee the conservation of the third component of the total spin.

F is composed of several kinematic factors and Clebsch–Gordan coefficients and is written as

$$F(L,\boldsymbol{l},\boldsymbol{j},\boldsymbol{j_z}) = \sum_{\nu_1,\nu_2} \langle \frac{1}{2}\ \nu_1 \frac{1}{2}\ \nu_2 | SS_z \rangle\ (-1)^{j_{z_1}+j_{z_2}-S_z} f_L(l_1, j_{z_1}-\nu_1, l_2, j_{z_2}-\nu_2, L, M) \tag{A.12}$$

with the definition of f_L given by

$$\begin{aligned} f_L(l_1, j_{z_1}-\nu_1, l_2, j_{z_2}-\nu_2, L, M) &= \hat{L}^{-1}(-1)^M\ \langle l_1\ 0\ l_2\ 0 | L\ 0\rangle \\ &\times \Big\{ \langle l_1 j_{z_1}-\nu_1 \tfrac{1}{2}\nu_1 | j_1 j_{z_1}\rangle\ \langle l_2 j_{z_2}-\nu_2 \tfrac{1}{2}\nu_2 | j_2 j_{z_2}\rangle\ \langle l_1\ j_{z_1}-\nu_1\ l_2\ j_{z_2}-\nu_2 | L\ M\rangle \\ &\quad - \langle l_1 j_{z_1}-\nu_2 \tfrac{1}{2}\nu_2 | j_1 j_{z_1}\rangle\ \langle l_2 j_{z_2}-\nu_1 \tfrac{1}{2}\nu_1 | j_2 j_{z_2}\rangle\ \langle l_1\ j_{z_1}-\nu_2\ l_2\ j_{z_2}-\nu_1 | L\ M\rangle \Big\}. \end{aligned} \tag{A.13}$$

In Eqs. (A.12) and (A.13), $\hat{l}$ is defined as $\hat{l} = \sqrt{2l+1}$, and the subtraction in Eq. (A.13) arises from the anti-symmetrization of the two neutrons.

On the other hand, the factor G^{ν} in Eq. (A.11) is determined by the radial wave function, and its explicit form becomes

$$\begin{aligned} G^{\nu}(L,\boldsymbol{n},\boldsymbol{l},\boldsymbol{j}) &= (\pi\nu)^{\frac{3}{4}} \hat{l}_1 \hat{l}_2\ (-2)^L \left(\sqrt{2}i\right)^{-(L+l_1+l_2)}\ (l_1+l_2+L+1)!! \\ &\times \sum_{j,a,b} g_j^{(L)} (\alpha_j^{(L)} - 2\nu)^{\frac{1}{2}(l_1+l_2-L)} \frac{C_a^*}{(\nu_a^*+\nu)^{l_1+\frac{3}{2}}} \frac{C_b^*}{(\nu_b^*+\nu)^{l_2+\frac{3}{2}}} \\ &\times \left[\frac{2\nu_a^*+\alpha_j}{\nu_a^*+\nu} + \frac{2\nu_b^*+\alpha_j}{\nu_b^*+\nu}\right]^{-\frac{1}{2}(l_1+l_2+L+3)}, \end{aligned} \tag{A.14}$$

where the parameters C_a, C_b, ν_a, and ν_b correspond to the expansion coefficients in the radial wave function of the single-particle orbit in Eq. (A.3). Here the superscript of the single-particle state (nlj) in the individual coefficients is omitted for simplicity. g_j and α_j are the expansion coefficients for the radial wave function in the cluster model with L, which is given in Eq. (A.6), while ν shows the internal width of the $2n$ cluster contained in Eq. (A.8).

A.3. Shell–cluster overlap by coordinate rearrangement

We can also calculate the shell–cluster overlap by employing the coordinate rearrangement, which is given by

$$\boldsymbol{R} = \frac{\boldsymbol{r}_1 + \boldsymbol{r}_2}{2} \tag{A.15}$$

$$\boldsymbol{\rho} = \boldsymbol{r}_1 - \boldsymbol{r}_2. \tag{A.16}$$

$\boldsymbol{R}$ represents the center-of-mass coordinate of the two valence neutrons, which is the same as the core–$2n$ relative coordinate in the present calculation, while $\boldsymbol{\rho}$ denotes their relative coordinate.

According to the relationship between Eqs. (A.15) and (A.16), we can directly calculate the overlap integral. The computational result on the basis of the coordinate rearrangement becomes

$$\langle \Psi_s | \Psi_c \rangle = 2 \sum_{\nu_1', \nu_2'} \langle l_1 j_{z_1} - \nu_1' \frac{1}{2} \nu_1' | j_1 j_{z_1} \rangle \langle l_2 j_{z_2} - \nu_2' \frac{1}{2} \nu_2' | j_2 j_{z_2} \rangle \langle \frac{1}{2} \nu_1' \frac{1}{2} \nu_2' | 00 \rangle \times \mathcal{M}^{(\nu_r)}(n_1, l_1, m_1', n_2, l_2, m_2', L) \tag{A.17}$$

with the abbreviation of $m_i' = j_{zi} - \nu_i'$. Here $\mathcal{M}^{(\nu_r)}$ is defined as

$$\mathcal{M}^{(\nu_r)}(n_1, l_1, m_1', n_2, l_2, m_2', L) = \left(\frac{2\nu_r}{\pi}\right)^{\frac{3}{4}} \sqrt{4\pi}\, \hat{L} \sum_{abj} C_a^* C_b^* g_j^{(L)} (-1)^{m_1' + m_2'} \hat{l}_1 \hat{l}_2 \times \sum_{\lambda_1 \lambda_2} \sqrt{\begin{pmatrix} 2L \\ 2\lambda_1 \end{pmatrix}} \left(\frac{1}{2}\right)^{\lambda_1 + \lambda_2} \sum_{\mu_1 \mu_2} \langle \lambda_1 \mu_1 \lambda_2 \mu_2 | LM \rangle \mathcal{K}^{(\nu_1, \nu_b, \nu_r, \alpha_j)}(l_1, \lambda_1, \mu_1, l_2, \lambda_2, j_{z_1}, \nu_1', j_{z_2}, \nu_2'), \tag{A.18}$$

where $\mathcal{K}$ contains the radial integration and $3j$ symbol as

$$\mathcal{K}^{(\nu_a, \nu_b, \nu_r, \alpha_j)}(l_1, \lambda_1, \mu_1, l_2, \lambda_2, j_{z_1}, \nu_1', j_{z_2}, \nu_2') = \sum_{\lambda \mu} (-1)^{\mu} \hat{\lambda}^2 \times \begin{pmatrix} l_1 & \lambda & \lambda_1 \\ 0 & 0 & 0 \end{pmatrix} \begin{pmatrix} l_1 & \lambda & \lambda_1 \\ -m_1' & -\mu & \mu_1 \end{pmatrix} \begin{pmatrix} l_2 & \lambda & \lambda_2 \\ 0 & 0 & 0 \end{pmatrix} \begin{pmatrix} l_2 & \lambda & \lambda_2 \\ -m_2' & \mu & \mu_2 \end{pmatrix} \times \mathcal{I}^{(\nu_a, \nu_b, \nu_r, \alpha_j)}(l_1, \lambda_1, l_2, \lambda_2, \lambda). \tag{A.19}$$

$\mathcal{I}$ is calculated from the double integration of the radial wave function, and its explicit form is

$$\mathcal{I}^{(\nu_a, \nu_b, \nu_r, \alpha_j)}(l_1, \lambda_1, l_2, \lambda_2, \lambda) = \sqrt{\frac{\pi}{2\beta r_1 r_2}} \int r_1^2 dr_1 \int r_2^2 dr_2 \times r_1^{l_1 + \lambda_1} e^{-(\nu_a^* + \nu_r + \frac{1}{4}\alpha_j) r_1^2} \mathcal{J}_\lambda(\beta_j r_1 r_2)\, r_2^{l_2 + \lambda_2} e^{-(\nu_b^* + \nu_r + \frac{1}{4}\alpha_j) r_2^2}, \tag{A.20}$$

which contains a modified Bessel function in the integrand:

$$\mathcal{J}_\lambda(x) = \sqrt{\frac{\pi}{2x}} J_{\lambda + 1/2}(x). \tag{A.21}$$

Here J denotes the normal Bessel function, and β_j is given by $\beta_j = 2\nu_r - \alpha_j/2$. In all of the expressions, the superscripts in parentheses, $(\nu_a, \nu_b, \nu_r, \alpha_j)$ in $\mathcal{K}$, represent the set of width parameters for the radial wave functions, while the variables in the arguments of the individual functions show the set of quantum numbers.

As can be understood from the final expression in Eq. (A.17), the overlap integral in the method of the coordinate rearrangement has the structure of multiple summations, in which the Clebsch–Gordan coefficients and the radial integration get entangled. The final expression of the overlap obtained by the coordinate rearrangement is much more complicated than the expression by the Fourier transformation in Eq. (A.11), which is given as the simple product of the angular momentum part and the radial integration part.

References

[1] P. Ring and P. Schuck, *The Nuclear Many-Body Problem* (Springer, Berlin, 2004), 1st ed.
[2] E. Caurier, G. Martínez-Pinedo, F. Nowacki, A. Poves, and A. P. Zuker, Rev. Mod. Phys. **77**, 427 (2005).
[3] T. Otsuka, A. Gade, O. Sorlin, T. Suzuki, and Y. Utsuno, Rev. Mod. Phys. **92**, 015002 (2020).
[4] N. Shimizu, T. Abe, M. Honma, T. Otsuka, T. Togashi, Y. Tsunoda, Y. Utsuno, and T. Yoshida, Phys. Scr. **92**, 063001 (2017).
[5] K. Ikeda, H. Horiuchi, and S. Saito, Prog. Theor. Phys. Suppl. **68**, 1 (1980).
[6] H. Horiuchi, K. Ikeda, and K. Katō, Prog. Theor. Phys. Suppl. **192**, 1 (2012).
[7] H. Horiuchi, Prog. Theor. Phys. Suppl. **62**, 90 (1977).
[8] K. J. Cook et al., Phys. Rev. Lett. **124**, 212503 (2020).
[9] Y. Kubota et al., Phys. Rev. Lett. **125**, 252501 (2020).
[10] K. Hagino and H. Sagawa, Phys. Rev. C **72**, 044321 (2005).
[11] Y. Kikuchi, K. Ogata, Y. Kubota, M. Sasano, and T. Uesaka, Prog. Theor. Exp. Phys. **2016**, 103D03 (2016).
[12] T. Yamada, Y. Funaki, H. Horiuchi, K. Ikeda, and A. Tohsaki, Prog. Theor. Phys. **120**, 1139 (2008).
[13] E. Hiyama, Y. Kino, and M. Kamimura, Prog. Part. Nucl. Phys. **51**, 223 (2003).
[14] S. Aoyama, S. Mukai, K. Katō, and K. Ikeda, Prog. Theor. Phys. **93**, 99 (1995).
[15] E. Hiyama and M. Kamimura, Phys. Rev. A **85**, 022502 (2012).
[16] E. Hiyama and M. Kamimura, Phys. Rev. A **85**, 062505 (2012).
[17] N. Shimizu, T. Mizusaki, Y. Utsuno, and Y. Tsunoda, Comput. Phys. Commun. **244**, 372 (2019).
[18] M. Moshinsky, Nucl. Phys. A **13**, 104 (1959).
[19] D. K. Maretis, J. Chem. Phys. **71**, 917 (1979).
[20] T. Fukui, L. De Angelis, Y. Z. Ma, L. Coraggio, A. Gargano, N. Itaco, and F. R. Xu, Phys. Rev. C **98**, 044305 (2018).
[21] A. T. Kruppa, G. Papadimitriou, W. Nazarewicz, and N. Michel, Phys. Rev. C **89**, 014330 (2014).
[22] H. Masui, K Katō, N. Michel, and M. Ploszajczak, Phys. Rev. C **89**, 044317 (2014).
[23] Y. Takenaka, R. Otani, M. Iwasaki, K. Mimura, and M. Ito, Prog. Theor. Exp. Phys. **2014**, 113D04 (2014).
[24] M. Iwasaki, R. Otani, Y. Takenaka, and M. Ito, Prog. Theor. Exp. Phys. **2015**, 023D01 (2015).
[25] M. Nakao, H. Umehara, S. Ebata, and M. Ito, Proc. 2017 Symp. Nuclear Data, p. 185 (2018).
[26] H. Friedrich, Phys. Rep. **74**, 209 (1981).
[27] Y. Utsuno, T. Otsuka, T. Mizusaki, and M. Honma, Phys. Rev. C **60**, 054315 (1999).
[28] M. Honma, T. Otsuka, B. A. Brown, and T. Mizusaki, Eur. Phys. J. A **25**, 499 (2005).
[29] M. Honma, T. Otsuka, T. Mizuaki, and M. Hjorth-Jensen, Phys. Rev. C **80**, 064323 (2009).
[30] M. Matsuo, K. Mizuyama, and Y. Serizawa, Phys. Rev. C **71**, 064326 (2005).
[31] K. Kaneko, N. Shimizu, T. Mizusaki, and Y. Sun, Phys. Lett. B **817**, 136286 (2021).